Conventions for CTA dark matter searches

Authors:

J. Rico (IFAE, Barcelona), F. Zandanel (U. Amsterdam), G. Zaharijas, C. Eckner (U. Nova Gorica), T. Bringman (U. Oslo), F Iocco (ICTP-SAIFR, São Paulo), M. A. Sánchez-Conde (IFT-UAM/CSIC, Madrid), M. Fornasa (GRAPPA, Amsterdam), M. Doro (U. Padova)

Keywords:

CTA, Software, Science, Data Analysis, Dark Matter, Conventions

Version History:

Ver.	Date	Comment	Distribution	Corresponding...
0.0	2015-10-26	First draft after Liverpool meeting	FUND WG conveners	
0.1	2017-06-01	Pre-release	Authors	
0.2	2017-06-27	DMEP first release with many open issues	DMEP WG	
0.3	2017-08-31	Includes the comments posted in the redmine forum; authors asked to solve open issues	Authors	
0.4	2017-10-27	Chapters revised by co-authors, no open issues left, for last check before release	Authors	
1.0	2017-11-03	First public release	CTA Consortium	

Table of Contents

1 Introduction

CTA will search for dark matter (DM) annihilation or decay signals from different objects, such as the Galactic center and halo, dwarf spheroidal galaxies (dSph), clusters of galaxies and others [1]. The DM analysis allows certain degrees of freedom, ranging from the used nomenclature and units to, more importantly, the methods to estimate the expected gamma-ray flux from a given source, or the statistical treatment of the data and/or simulations. Expectedly, different analyzers would by default take independent decisions about all these choices. Therefore, in order to homogenize CTA DM results, allowing an easy and direct comparison of the results of the different analyses and, eventually, their combination in a common global DM search, it is desirable to agree beforehand in a common set of standard choices.

In this document we propose general guidelines to be followed in all CTA DM analyses during the construction and science periods. Some of the provided guidelines can be trivially fulfilled (e.g. nomenclature, use of certain DM profiles), whereas others depend on the work of third parties (e.g. features of the analysis codes or of the simulations used for the computation of the instrument response) and may be very difficult or impossible to fulfill. For the latter cases, the provided guidelines serve a double purpose: first they can be used for the communication of the Dark Matter and Exotic Physics (DMEP) working group (WG) needs to the relevant third parties; second, analyzers should still follow them as much as possible and explain where and why divergences from them remain.

2 Definitions, nomenclature and units

In this section we define all concepts needed for CTA DM analysis, and present the nomenclature and units used throughout the rest of the document, and recommended for CTA DM analyses and publications. When introducing physical quantities, we shall use the following format:

- **Name of physical quantity** – nomenclature – [units] – Brief definition/explanation.

On the other hand, when introducing concepts, we shall do it using the following format:

- **Name of concept** – Brief definition/explanation.

2.1 Physical and estimated variables

- **Energy** or **True energy** – E – [TeV] – True energy of a gamma ray.
- **Estimated energy** – E' – [TeV] – Estimated energy of a gamma-ray candidate.
- **[Incoming or true] direction** – $\bar{P}$ – ([deg],[deg]) or ([hh:mm:ss],[deg]) – Incoming direction of a gamma ray or, in general, point in the sky. It can refer to an absolute direction in a given reference frame, or be the relative direction with respect to another reference direction (typically, the pointing or source directions, see below).
- **[Telescope] pointing direction** – $\bar{P}_{\rm tel}$ – ([deg],[deg]) or ([hh:mm:ss],[deg]) – direction in the sky where the telescopes are pointing. It can be replaced by the center of the observed field of view if the pointing direction is different for different telescopes (e.g. during divergent pointing).
- **Source direction/position/coordinates** – $\bar{P}_{\rm src}$ – ([deg],[deg]) or ([hh:mm:ss],[deg]) – direction in the sky where a possible gamma-ray source of interest (or, for extended sources, its center) is located.
- **Estimated [incoming] direction** – $\bar{P}'$ – ([deg],[deg]) or ([hh:mm:ss],[deg]) – Incoming estimated direction of a gamma ray candidate. It can refer to an absolute direction in a given reference frame, or be the relative direction with respect to another reference direction (typically, the pointing or source directions).

- **Offset angle** – Ψ – [deg] – Angular distance of the incoming direction of a gamma ray to the pointing direction, i.e. $\Psi = |\bar{P} - \bar{P}_{\rm tel}|$ (useful when radial symmetry around the telescope pointing direction can be assumed).
- **Estimated offset angle** – Ψ' – [deg] – Angular distance of the estimated incoming direction of a gamma-ray candidate to the pointing direction, i.e. $\Psi = |\bar{P}' - \bar{P}_{\rm tel}|$.
- **Angular distance to source center** – θ – [deg] – Angular distance of the estimated incoming direction of a gamma-ray candidate to the source center, i.e. $\theta = |\bar{P}' - \bar{P}_{\rm src}|$.
- **Observation time** – $T_{\rm obs}$ – [s] – Total effective observation time (i.e. removing bad runs, dead time, etc).

2.2 Analysis

- **Signal region** or **ON region** or **region of interest (ROI)** – For a given analysis, subset of events passing all signal selection cuts (including those on $\bar{P}'$ and E').

  The term "ON region" is used for analyses with background estimation from control region(s) (see Section 6.1.1), whereas for global model fitting analyses (see Section 6.1.2) we use the term "ROI".
- **Background control region** or **OFF region** – For a given ON region in analyses with background estimation from control region(s), the OFF region is the complementary subset of events passing all signal selection cuts except for that on $\bar{P}'$. Instead, we select events with $\bar{P}'$ within a region of zero (or computable) signal intensity, and from which the number of residual background events in the ON region can be estimated (see below). The OFF region is often (but not necessarily) observed simultaneously or contemporaneously with the ON region.

  When a suitable OFF region cannot be defined, as for example the Galactic diffuse emission at the Galactic center, the background must be estimated from theoretical models (see 6.1.2 for more details).
- **OFF/ON acceptance ratio** – τ – [1] – In analyses with background estimation from control region(s), τ is the ratio of acceptances of the OFF and ON regions. (E.g. τ would be 2 for an OFF region of the same size as the ON, observed for double the time, or for an OFF region of double size observed during the same time.)
- **Number of signal events [in the signal region]** – g – [1] – Mean number of signal events (normally gamma rays coming from the source under study) in the signal region. g is the quantity we intend to estimate or constrain with our observations, and can be normally computed under a hypothesis for its morphological and spectral distributions, and knowing the response of the detector (see Section 2.3).
- **Number of [residual] background events [in the signal region]** – b – [1] – Mean number of background events (normally charged cosmic rays and gamma rays from additional sources different from the one under study) in the signal region.
- **Number of observed events [in the signal region]** – $N_{\rm ON}$ or N – [1] – Number of observed events in the signal region (ON region or ROI). $N_{\rm ON}$ or N is a Poisson-distributed random variable with mean $g + b$.
- **Number of observed OFF events** – $N_{\rm OFF}$ – [1] – Number of observed events in the OFF region. $N_{\rm OFF}$ is a Poisson-distributed random variable with mean τb.

2.3 Instrument Response Function (IRF)

The instrument response function (IRF) encodes the information needed for computing the expected event rates measured by the telescope (vs. estimated energy, estimated energy and time), when observing a given gamma-ray flux (vs. energy, direction and time). Conversely, given measured event rates the IRF allows us to estimate the original physical flux. The IRF is composed essentially of the

probability density functions (PDFs) for energy and arrival direction, plus gamma-ray collection area and residual background rates.

(Note: At least for prospective analyses we shall assume radially symmetric IRFs with respect to the pointing direction of the telescope response, i.e. the $\bar{P}$ and $\bar{P}'$ dependences shall be simplified by dependences on Ψ and Ψ', respectively.)

- **Energy resolution function** – $f_E(E' \mid E, \bar{P})$ – [1] – PDF of the energy estimator.

  f_E depends (at least) on E, $\bar{P}$, the analysis cuts and the observational conditions (zenith, weather, intensity of night-sky-background (NSB) light, ...).

- **Migration Matrix** – A 2D (E' vs E) histogram describing f_E for a given value of $\bar{P}$.

- **Spatial resolution function** – $f_{\bar{P}}(\bar{P}' \mid E, \bar{P})$ – [1] – PDF of the direction estimator.

  $f_{\bar{P}}$ depends (at least) on E, $\bar{P}$, the analysis cuts and the observational conditions (zenith, weather, NSB, ...).

- **Angular resolution** – $\sigma(E, \bar{P})$ – [deg] – width of a symmetric 2D Gaussian centered at $\bar{P}$ often used to approximate $f_{\bar{P}}$, for given values of E and $\bar{P}$.

- **Effective [collection] area** – $A_{\rm eff}(E, \bar{P})$ – [cm^2] – Given a surface of area $A_{\rm tot}$ perpendicular to the pointing direction and sufficiently large so that any gamma ray of energy E and incoming direction $\bar{P}$ that does not cross $A_{\rm tot}$ has negligible probability of being detected, then $A_{\rm eff} = \epsilon \times A_{\rm tot}$ with ϵ being the overall detection efficiency for gamma rays crossing $A_{\rm tot}$.

  $A_{\rm eff}$ depends (at least) on E, $\bar{P}$, the analysis cuts and the observational conditions (zenith, weather, NSB, ...).

- **[Estimated residual] background rate** – $\frac{d\hat{b}}{dtdE'd\bar{P}'}$ – [s^{-1} TeV^{-1} sr^{-1}] – Estimated residual rate of background events in the signal region.

  $\frac{d\hat{b}}{dtdE'd\bar{P}'}$ depends on E', $\bar{P}'$, the analysis cuts and the observational conditions (zenith, weather, NSB, ...).

  For real observations, $\frac{d\hat{b}}{dtdE'd\bar{P}'}$ is commonly approximated by the histogram of event rates in the background control region, i.e.:

$$\frac{d\hat{b}}{dtdE'd\bar{P}'} \simeq \frac{N_{\rm OFF}(\Delta E', \Delta \bar{P}')/\tau}{T_{\rm obs}\Delta E' \Delta \bar{P}'} \tag{1}$$

  where $N_{\rm OFF}(\Delta E', \Delta \bar{P}')$ is the number of events observed in the OFF region, with measured incoming direction in the region $\Delta \bar{P}'$ and measured energy in the interval $\Delta E'$. Note that this expression is valid both for analyses with background estimation from background control region (to estimate the total background) and from global model fit (to estimate the cosmic ray background, see Section 6.1.2, and Equation 18).

2.4 Gamma-ray flux

- **Average annihilation or decay spectrum** – $\frac{dN}{dE}$ – [TeV^{-1}] – Average gamma-ray spectrum per DM annihilation or decay reaction.

- **DM density profile** – $\rho(r)$ – [GeV cm^{-3}] – DM density expressed as a function of the distance r to the center of a given DM halo (e.g. Galactic center, dSph, galaxy cluster, ...), assuming radial symmetry.

- **Differential astrophysical factor or J-factor** – $\frac{dJ}{d\Omega}$ ($\frac{dJ_{\rm ann}}{d\Omega}$ or $\frac{dJ_{\rm dec}}{d\Omega}$) – [GeV^2 cm^{-5} sr^{-1}] or [GeV cm^{-2} sr^{-1}] – For a DM density profile at a given distance from Earth, the differential J-factor is proportional to the gamma-ray intensity produced by DM annihilation or decay, arriving from the direction $\bar{P}$. In the case of annihilation, it is computed as:

$$\frac{dJ_{\rm ann}}{d\Omega}(\bar{P}) = \int_{\rm l.o.s.} dl\, \rho^2(l, \bar{P}) \quad , \tag{2}$$

where the integral runs over line-of-sight (l.o.s.) through the DM distribution for a direction $\bar{P} \in d\Omega$. In the case of decay the differential J-factor is computed as:

$$\frac{dJ_{\rm dec}}{d\Omega}(\bar{P}) = \int_{\rm l.o.s.} dl\, \rho(l, \bar{P}) \quad , \tag{3}$$

- **Astrophysical factor or J-factor** – J ($J_{\rm ann}$ or $J_{\rm dec}$) – [GeV^2 cm^{-5}] or [GeV cm^{-2}] – $\frac{dJ}{d\Omega}$ integrated in a given sky region($\Delta\Omega$):

$$J(\Delta\Omega) = \int_{\Delta\Omega} d\Omega' \, \frac{dJ}{d\Omega'} \quad . \tag{4}$$

- **Gamma-ray differential flux** – $\frac{d\Phi}{dE\, d\Omega}$ – [cm^{-2} s^{-1} TeV^{-1} sr^{-1}] – Number of gamma rays per unit time, area and energy arriving at a given location (normally, at Earth) from a given direction.

  If the gamma rays are produced by DM annihilation, the differential flux is given by:

$$\frac{d\Phi}{dE\, d\Omega} = \frac{1}{4\pi} \frac{\langle \sigma v \rangle}{k\, m_{\rm DM}^2} \frac{dJ_{\rm ann}}{d\Omega} \frac{dN}{dE} \quad , \tag{5}$$

  with $\langle \sigma v \rangle$ ([cm^3 s^{-1}]) being the **thermally averaged annihilation cross-section**; $k = 2$ ($k = 4$) for Majorana (Dirac) DM particles; and $m_{\rm DM}$ ([TeV]) the **DM particle mass**. Also note that this factorization is only valid if $\langle \sigma v \rangle$ is velocity independent (i.e. not in the presence of Sommerfeld effect).

  Conversely, if the gamma rays are produced by DM decay, the differential flux is given by:

$$\frac{d\Phi}{dE\, d\Omega} = \frac{1}{4\pi} \frac{1}{\tau_{\rm DM} m_{\rm DM}} \frac{dJ_{\rm dec}}{d\Omega} \frac{dN}{dE} \quad , \tag{6}$$

  with $\tau_{\rm DM}$ ([s]) the **DM particle lifetime**.

3 dN/dE

3.1 General

To lowest order in perturbation theory, DM can annihilate or decay into pairs of standard model (SM) leptons, quarks or electroweak gauge bosons. For the latter two channels, the fragmentation and/or decay of the final states leads to essentially universal (i.e. very similar) gamma-ray spectra, dominated by the decay of neutral pions, $\pi^0 \to \gamma\gamma$. Gamma-ray spectra from lepton final states, on the other hand, look qualitatively different; the reason is a suppressed production of π^0 (which is anyway only possible for $\tau^\pm$ final states) such that large contributions to the spectrum arise from final state radiation (FSR) in lepton decays, $\tau^\pm \to \mu^\pm + \gamma$ ($+\nu$s) and $\mu^\pm \to e^\pm + \gamma$ ($+\nu$s). For each 2-body final state, i.e. a pair of on-shell particles emitted back-to-back, the resulting gamma-ray yield dN/dE is uniquely defined. In this sense, **two-body final states are model-independent** and the underlying particle model only enters by specifying the branching ratios into the respective channels.[1] Note that this is true also for 2-body final states which do not exist at tree-level, notably those containing at least one photon (and hence giving rise to monochromatic 'line' signals).

Going beyond leading order, one encounters not only 'loop contributions' but three or more particles in the final state of DM annihilation or decay. Because the kinematics is not fixed as in the 2-body case, a given annihilation process, e.g. $\chi\chi \to \tau^+\tau^-\gamma$, is not uniquely described by just one number (i.e. the partial cross section, or branching ratio) but one must additionally specify the angular and/or energy distribution of the final states in order to obtain the expected gamma-ray spectrum. This can vary greatly, depending on the underlying model. In this sense, **three-body final states are highly model-dependent**. For the case of $\tau^+\tau^-\gamma$, for example, it makes a very clear difference for the resulting gamma-ray spectrum whether the process is dominated by FSR (as for Kaluza-Klein DM [3]) or by

[1] Strictly speaking, this statement only remains true if one also specifies the polarization states of electroweak gauge bosons (longitudinal or transverse). The difference in terms of the resulting gamma-ray spectrum, however, is relatively small [2].

'virtual internal bremsstrahlung' (VIB, as it appears in models with Majorana DM [4]): in the first case, the spectrum is described by a sharp cutoff, while in the second it is closer to a monochromatic line. Also $W^+W^-\gamma$ final states can produce line-like spectra [5]. Quark final states on the other hand – with the exception of $\bar{t}t$, which is more difficult to model – are examples of channels that suffer from relatively little model dependence even when taking into account QCD corrections: The gamma-ray spectrum from $\bar{q}qg$ final states varies by less than a factor of 2 at all energies between the most extreme cases for the underlying model realizations [6].

A widely used way to incorporate electroweak corrections to the dN/dE from the various SM "two-body final states" is the one provided by Cirelli et al. [7], and this is the one that CTA analysis will (mostly) follow as well. As this refers to adding one Z or $W^\pm$ to the final states,[2] however, it is important to be aware that all general remarks of the previous paragraph apply. In particular – rather than being 'model-independent', as this approach is sometimes referred to – these spectra do in general *not* capture the following situations:

- DM that is not an electroweak singlet, like Higgsino or Wino DM, because initial state radiation (ISR) is not taken into account.
- Models in which VIB contributions are relevant. One of the most important examples in practice is Majorana DM, like SUSY neutralinos, annihilating to fermions much lighter than the DM particle (see the detailed discussion in [9], in particular Fig. 15)
- DM much heavier than 10 TeV, because then higher-order electroweak corrections would have to be taken into account even under the same assumptions that went into deriving these spectra (missing 'resummation of leading logarithms')

While this may seem to be a long list, there are of course also many situations where the spectra provided in [7] *are* a very good approximation to what is expected from the underlying particle physics model. In particular, this is the case for (almost) contact-interactions, as described e.g. by effective operators, or for quark final states in general (see above).

Apart from these uncertainties in the gamma-ray spectra due to the underlying particle physics model, it has been pointed out that there are further significant **uncertainties due to the choice of event generators** like Pythia or Herwig (see, e.g. [10]). These uncertainties are largest, however, at energies too low or too high to be relevant from the point of view of indirect detection with CTA (this comment refers to typical '$b\bar{b}$-like' spectra that are strongly suppressed with respect to the background both for $E_\gamma \gtrsim m_{\rm DM}$ and for $E_\gamma \ll m_{\rm DM}$). In the relevant energy range, at around 20% of the DM mass and below, these uncertainties are instead typically smaller than those deriving from the background determination and the underlying particle models, and we will therefore not address them explicitly in the following.

3.2 Input for analysis

Given the need for more or less unified reference spectra in the literature, we recommend CTA analyses to use the dN/dE functions for DM annihilation or decay into 'single SM pairs' (in fact 3-body final states) as computed by Cirelli et al. [7] – but also to clearly comment in your publications the drawbacks / limitations associated to this approach when it comes to interpreting the results. These spectra are available in different machine-readable formats at: https://portal.cta-observatory.org/WG/PHYS/SitePages/Dark%20Matter%20and%20Exotic%20Physics%20SWG.aspx.

CTA analyses shall provide results for DM masses between 10 GeV and 100 TeV for the $b\bar{b}$ final states as reference, given that the gamma-ray spectrum for this channel is particularly model-independent (see the above discussion, but also the fact that, for this channel, the dN/dE from [7] is essentially indistinguishable from taking the uncorrected 2-body result directly from Pythia).

It is also desirable to complement these results by including (in this order of priority) the channels W^+W^-, $\tau^+\tau^-$ and $\mu^+\mu^-$. For these channels we recommend to show results for DM masses larger than

[2] Technically, it follows the approach of Ciafaloni et al. [8] to compute final state radiation of these particles; the fragmentation of the three final state particles is then done with Pythia version 8.135.

10 TeV using a different line style (e.g. dashed instead of solid), and to include in the plot explanation the caveats applying to those results, i.e. that the used spectra are inconsistent with the assumptions under which they were derived, and how they are provided mainly for comparison of sensitivity with previously published results.

In addition, we suggest authors to consider complementing (not necessarily in the final results plot) the W^+W^-, $\tau^+\tau^-$ and $\mu^+\mu^-$ results with the corresponding ones obtained using the lowest-order (i.e. proper 2-body) Pythia spectra (also available at https://portal.cta-observatory.org/WG/PHYS/SitePages/Dark%20Matter%20and%20Exotic%20Physics%20SWG.aspx), in order to allow a straight-forward comparison with results in the literature, and to illustrate the impact of the implemented electroweak corrections.

Whenever CTA limits on specific DM models are derived, an effort should be made to use the actual photon spectrum in the respective model (by either deriving it or by taking it from the literature). Only in cases where this is not feasible – e.g. due to computer time limitations in large parameter scans of complex DM models – it should be attempted to approximate the full spectrum as a linear combination of the reference dN/dE curves for the available channels. In any case, the exact procedure should be briefly discussed beforehand with the DMEP WG.

As a general rule, spectral lines shall be studied using the guidelines presented in this document, considering that $\frac{dN}{dE} \propto \delta(E - E_0)$, with E_0 being the energy of the line. For instance, for DM annihilation into $\gamma\gamma$: $\frac{dN}{dE} = 2\delta(E - m_{\rm DM})$; and for the $Z\gamma$ channel: $\frac{dN}{dE} = \delta(E - m_{\rm DM}(1 - m^2_{\rm DM}/4m^2_Z))$. Given the strong theoretical motivations, it is also desirable to use further templates to search for other sharp ('smoking gun') spectral features, e.g. the one associated to VIB or a box-shaped spectrum.

4 Astrophysical factor

4.1 General considerations

For the computation of the J-factors of particular observational targets we shall observe the following general rules, which apply to all kind of targets unless otherwise stated.

- Choice of the DM density profile. Several parameterizations exist in the literature. By default, we will use one or several of the following density profiles:
  - **Generalized Navarro-Frenk-White** (gNFW, e.g. [11]) profile:

$$\rho(r) = \frac{\rho_c}{\left(\frac{r}{r_s}\right)^{\gamma}\left(1+\frac{r}{r_s}\right)^{3-\gamma}} \quad , \tag{7}$$

    with the values of the **characteristic density** ρ_c, **scale radius** r_s and the index γ depending on the considered halo.
  - **Navarro-Frenk-White** (NFW, [12]) profile, obtained by taking $\gamma = 2$ in Equation 7.
  - **Einasto** profile [13, 14]:

$$\rho(r) = \rho_c e^{-\frac{2}{\alpha}\left(\left(\frac{r}{r_s}\right)^{\alpha}-1\right)} \quad , \tag{8}$$

    with the values of the scale radius r_s, the characteristic density ρ_c and the index α depending on the considered halo.
  - **Isothermal** profile [15]:

$$\rho(r) = \frac{\rho_c}{1+\left(\frac{r}{r_s}\right)^2} \quad , \tag{9}$$

    with scale radius r_s and characteristic density ρ_c depending on the considered halo.

  When selecting the DM density profile in our analyses, it is important to follow two criteria: i) to use DM density models that can be compared to those used in gamma-ray community and ii) to use models which are state-of-the-art (if they differ from point i).

- Possible deviations from spherical symmetry. As first-order rule, we will consider spherically symmetric profiles. However, in cases for which non-sphericity is known to make a difference in the value of the J-factor, we shall include its effects. We can differentiate between two cases. i) Cases where we know the structure in detail and that it significantly deviates from spherical symmetry, e.g., as for some galaxy clusters (see below). ii) Cases where adopting a priori modeling profile including possible asymmetries can affect the final result, for which we shall consider this as a source of systematic uncertainty. See References [16, 17, 18] as starting point on this last issue for dwarf spheroidal galaxies (dSphs) and Reference [19] for the Milky Way.

- Impact of the unknowns involved in the mass reconstruction as, e.g., the number of member-stars with measured radial velocity or the velocity anisotropy for dSphs, or the hydrostatic mass bias for clusters. When possible, their effect shall be quantified. The best approach consists in including the effect of these uncertainties in the likelihood function as additional nuisance parameters. Alternatively, one can show the effect of the statistical scatter around the best-fit parameters (e.g., ρ_c and r_s) of the available state-of-the-art models in the exclusion plots. Finally, if none of the above approaches is possible, we shall at least bracket the real value to the best of our knowledge by making different assumptions.

- Amount of substructures. Depending on the target, the existence of substructures within the DM halos can make a big difference in the J-factor for DM annihilation, with respect to the values obtained assuming a completely smooth halo ($\bar{J}_{\rm ann}$). The effect is specially important for clusters of galaxies and close-by galaxies. Its relevance will be marginal for satellite galaxies due to tidal stripping [20]. Substructure treatment should include three scenarios: 1) a conservative minimal benchmark model with no substructures, 2) a realistic scenario with minimum halo mass $10^{-6} M_\odot$ and index of the sub-halo mass function $\alpha = 1.9$, and 3) an optimistic scenario with minimum halo mass $10^{-6} M_\odot$ (note that this does not affect much as the concentration-mass relation becomes flat at low masses) and $\alpha = 2$. In the latter two scenarios, the substructure boost should be computed following Eq. (18) and Table 3 of Ref. [20]. Additionally, the text should also mention the caveat that the value of $10^{-6} M_\odot$ is just a convention and it is not entirely justified at the moment (see, e.g., Ref. [21]).

  We shall parametrize this effect in terms of a multiplicative "boost factor" (B) applied to the smooth J-factor ($\bar{J}_{\rm ann}$), i.e.:

  $$J_{\rm ann} = (1 + B)\bar{J}_{\rm ann} \, . \tag{10}$$

  Note that this expression does not possess any radial information but it refers instead to the total, integrated boost. Should we need a radial description of subhalos (e.g., for targets that CTA may resolve spatially, or for specific studies on spatial properties of the DM signal), two different descriptions for the number density of subhalos as a function of distance to the host halo center should be adopted, namely the so-called i) "anti-biased" and ii) biased distributions, i.e., those where the subhalo number density is anti-correlated or follows, respectively, the smooth DM density profile of the host halo. Parametric expressions for both spatial prescriptions can be found in Equations (4) and (5) of Ref. [22]. These parameterizations were derived from state-of-the-art N-body cosmological simulations.

  As a general rule, we shall always study the case $B = 0$ (i.e., no deviation from smooth halo), plus the case of substructure, when relevant (see below comments for particular class of targets), obtaining the value of B from state-of-the-art studies done in-house or from the literature.

- Effect of baryons. When relevant, we shall consider the effect on the J-factor of the interaction between dark matter and baryonic matter. There are different possible ways to tackle this issue. The simplest, recommended approach consists in using all those profiles listed at the beginning of this subsection, explicitly mentioning in the text that the (yet uncertain) effect of baryons on the DM density profile is expected to be encapsulated within the uncertainties obtained from using such a set of diverse profiles. A more sophisticated analysis could, e.g., follow the work in Ref. [23], which relates the inner shape of the DM density profile with the ratio between stellar and halo mass in the particular object under study. We recommend to cite the latter work in any case (even if the most simple approach described above was adopted).

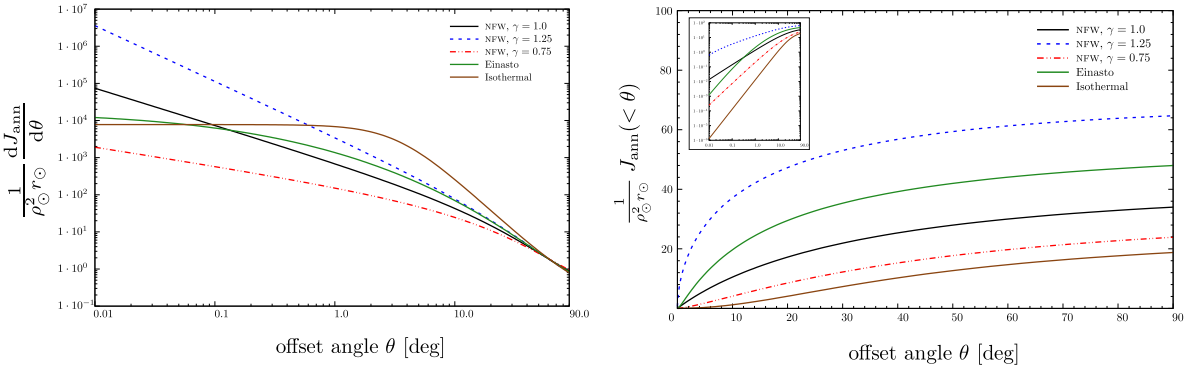

Figure 1 – J-factor as a function of the angular distance to the Galactic center for the DM density profiles listed in Section 4.2. Left panel shows $\frac{dJ_{\mathrm{ann}}}{d\theta}$ as a function of the offset angle with respect to the (θ), i.e., the "differential J-factor", while right panel shows its integrated value up to θ.

4.2 Choices for particular targets

- Galactic center and halo. Here we list a set of profiles which shall be used as benchmark options for CTA analyses (see also Figure 1):

  1. NFW profile with r_s = 20 kpc and local DM density ρ(8.5 kpc) = 0.4 GeV/cm^3.
  2. Einasto profile with r_s = 20 kpc, ρ(8.5 kpc) = 0.4 GeV/cm^3 and α = 0.17.
  3. Isothermal profile with r_s = 5 kpc and ρ(8.5 kpc) = 0.4 GeV/cm^3.
  4. gNFW profile with r_s = 20 kpc, ρ(8.5 kpc) = 0.4 GeV/cm^3 and γ = 1.25.
  5. gNFW profile with r_s = 20 kpc, ρ(8.5 kpc) = 0.4 GeV/cm^3 and γ = 0.75.

  Models 1-3 have been used by the Fermi-LAT collaboration, (see, e.g., [24]) and are comparable to those used by the H.E.S.S Collaboration [25, 26], whereas 4 and 5 are useful to bracket our uncertainty on those profiles – as from the latest observational determinations [27, 11] – and hence on the results of our DM analysis.

- dSphs. For the sake of a meaningful comparison and/or combination of DM searches, it is mandatory that J-factors for every dSph studied with CTA are computed using common method and assumptions. Several articles in the literature (see, e.g., Refs. [28] and [29]) present comprehensive lists reporting values of J-factors for all known dSphs at the moment of publication, using a coherent method, and could be in principle used for this purpose.

  However, there might be two problems related to the indiscriminate use of these results. First, as shown by Equations (5) and (6), and later in (15), the input we need for the analysis is the *differential* J-factor $\frac{dJ}{d\Omega}$, whereas often these articles only contain values of the J-factor integrated in a predefined region. Second, since new dSphs are currently being discovered by the present generation of optical survey instruments, it is possible that a consistent J-factor computation for all known dSph does not exist at every given time (at the same time, future, more sensitive optical studies can help better determine the stellar content of dSphs).

  Because of these reasons, we recommend to produce in-house J-factor calculations, whenever possible, for which the use of public codes such as CLUMPY [30] is recommended. Alternatively, we recommend to use values from the literature that have been computed using a coherent method for all considered dSphs, and whenever neither of these possibilities are feasible, we shall clearly discuss the consequences of the different approaches in the J-factor computation with respect to the comparison or combination of results.

  To quantify the systematic uncertainties we shall compare the results that are obtained when the J-factors are computed using a different set of assumptions or, ideally, the standard deviation of a set of different computations using different assumptions. For the latter case it might be useful to rely on compilations of results like the one presented in Ref. [31] (Fig. 7) or on studies about the effect in J of different systematic uncertainties (e.g., Refs. [32, 33]).

In addition, for dSphs it is mandatory to take into account the statistical uncertainty of the J-factor (see Section 6, Ref. [34] and Equation 13), particularly when combining/comparing results from different dSphs [35]. These uncertainties strongly depend on the particularities of the target, mainly on the number of available stars for the J-factor calculation. In general, classical dSphs have many (thousands) identified star members, whereas for the ultra-faint dSphs there are sometimes just a handful, which is reflected in a larger uncertainty in the J-factors.

- Galaxy clusters. The benchmark results should be presented using a standard NFW profile and an Einasto profile. Both the NFW and Einasto profile quantities should be derived from the mass (or, alternatively, radius) of a given cluster by adopting the proper concentration values for such mass as derived in Ref. [36] from N-body cosmological simulations. Note that we remain intentionally vague on the precise definition of the mass and radius: it can be virial, or defined with respect to the critical density.

  When the cluster under study is particularly disturbed, i.e., far from virialization like the Virgo cluster [37], a more complex DM profile matching such peculiarities should be considered. This is true also where there are available observational studies that reveal increased complexities on top of a theoretically smooth DM density profile, such as the case of the weak-lensing observed substructures in the Coma cluster [38, 39]. In general, deviations from spherical symmetry should be taken carefully into consideration as they could have a large impact on the final results, particularly for the case of DM decay, and should be discussed and agreed within the DMEP WG.

  The main uncertainties for clusters come from: 1) the mass determination of a given object, 2) the mass-concentration relation, and 3) the treatment of substructures in the case of DM annihilation. For the last point, we refer to the general considerations at the beginning of Section 4.1. Regarding the first point, the impact of masses obtained through different methods (e.g., weak lensing, Sunyaev-Zel'dovich effect, X rays) and their inherited biases (e.g., the hydrostatic mass bias in the X-ray determinations) should be investigated when possible. The uncertainties in the mass-concentration relation are a more complex matter. The scatter around this scaling relation amounts typically to 0.1 dex. However, the relation that refers only to relaxed halos differs significantly from the one that includes also non-relaxed halos at the mass scale of clusters of galaxies [36]. If a given object can be clearly identified as relaxed or not, the latter uncertainty can be neglected by adopting the proper scaling relation. Otherwise, our benchmark choice is to use the relation for relaxed halos (in general in better in agreement with observations), and consider the other choice (the relation including non-relaxed) as a source of systematic uncertainty. On the other hand, should detailed observational studies on this topic become available for a given cluster, these should be carefully considered against the mass-concentration relations derived from N-body simulations.

- Other targets (e.g., Large Magellanic Cloud, M31). We recommend authors to use the profiles outlined above (i.e., NFW, Iso, Einasto) when parameters can be found in literature. In the case of M31, for example, such parameter sets are available in Ref. [40]. For other objects not included in the previous list, a proposal for the J-factor computation, using the general guidelines outlined here, should be addressed by the authors and discussed within the DMEP WG.

5 IRF

5.1 Input for analysis

It has been proposed that all CTA observational data will be distributed with the corresponding Monte Carlo simulations necessary for the analysis, including IRF (f_E, $f_{\bar{P}}$, $A_{\rm eff}$ and $\frac{d\hat{b}}{dtdE'd\bar{P}'}$). In that case, there will be no special needs for DM-related analyses.

For prospective studies, we shall make use of IRFs for the following different configurations:

- North and South arrays. Final array configurations in the final geographical sites, including the correct magnetic fields. For each considered target, we shall assume the IRF for the array (North or South) providing a better sensitivity.

Target	Obs. time [h]
Galactic center/halo	525 + 700 (in case of detection)
dSphs	300 + 1050 (in case of detection)
Perseus cluster	300
LMC	340

Table 1 – Expected observations times ($T_{\rm obs}$) per DM target according to the CTA Science Case TDR [1].

- Zenith angle range. For each considered target we shall use the IRF corresponding to the zenith angle range for which observations can reasonably take place, taking into account the geographical location of the CTA site(s) and target coordinates.
- Nominal observation conditions. Nominal weather, NSB and hardware conditions shall be considered.
- Spectral and spatial dependences. We need the IRF as a function of E and $\bar{P}$ or Ψ (for f_E, $f_{\bar{P}}$ and $A_{\rm eff}$) or as a function of E' and $\bar{P}'$ or Ψ' (for $\frac{d\hat{b}}{dtdE'd\bar{P}'}$).

For the generation of IRFs for prospective studies we shall use the latest Monte Carlo production fulfilling these requirements.

The assumed observation times per target ($T_{\rm obs}$) shall be those included in the Science Case TDR [1], which are summarized in Table 1. For targets not included in this list, we recommend assuming a total observation time that allows a direct comparison with existing or planned results. Analyzers shall discuss the choice of $T_{\rm obs}$ for new targets in advance with the DMEP WG conveners.

5.2 Associated uncertainties

All IRF elements (f_E, $f_{\bar{P}}$, $A_{\rm eff}$ and $\frac{d\hat{b}}{dtdE'd\bar{P}'}$) are affected by statistical and systematic uncertainties, since they are estimated from finite-statistics MC simulations or datasets, and a full calibration of the detection chain is not possible.

The uncertainties in the background estimation ($\frac{d\hat{b}}{dtdE'd\bar{P}'}$) are specially relevant, since they enter directly the computation of the significance of a potential source detection, and should therefore be considered both for prospective and real data analyses. The likelihood functions described in Section 6 include these uncertainties in different ways depending on the type of analysis:

- For analyses with background estimation from a control (OFF) region (see Section 6.1.1), the statistical uncertainties in the background estimation are automatically taken into account with the inclusion of the b_{ij} and τ_{ij} nuisance parameters. These uncertainties depend on the size of the background control sample and the precision on the estimation of the normalization factor with respect to the signal (ON) region.

  The systematic uncertainty, on the other hand, can be parameterized through an extra component to σ_τ (i.e. the uncertainty of the τ_{ij}) as detailed in Equation 14, with $\sigma_{\tau,\rm sys} = 0.01 \cdot \tau_{\rm obs}$, following the criterium used in Monte Carlo sensitivity studies [41].

  The statistical and systematic uncertainties are proportional to $\sqrt{N_{\rm ON}}$ and $N_{\rm ON}$, respectively. Above a few 10^4 events, the systematic uncertainty becomes dominant. Since DM analyses typically involve much larger statistics, it is mandatory that they include systematic uncertainties.
- For analyses with background estimation from a global model fit the uncertainty for each background component should be specified by the respective models. Section 6.1.2 describes in detail how the uncertainties are included for the case of the analysis of the Galactic center region.

There are additional statistical and systematic uncertainties affecting f_E, $f_{\bar{P}}$ and $A_{\rm eff}$, which shall be considered in the analysis of real data, and particularly in the case of a positive detection, when we will

be able to provide estimations for fundamental Physics parameters such as the DM mass, annihilation cross section or decay lifetime. In such case, we shall consider at least:

- The statistical uncertainty of the different IRF elements caused by the finite statistics of the MC sample used in their determination.
- The systematic uncertainty in the absolute energy scale (related to how many Cherenkov photons are collected for a given particle shower). CTA requires a maximum uncertainty of 15% on this quantity [42]. The effect of this uncertainty shall be determined by comparing the results obtained when IRFs are computed using MC samples with nominal and $\pm$15% values of the number of detected Cherenkov photons, processed using the nominal analysis in terms of particle ID, energy and direction estimators.

  An alternative to estimate the effect of this uncertainty consists in introducing an extra bias in the energy dependence of f_E, $f_{\bar{P}}$ and $A_{\rm eff}$ during the data analysis (and not during MC generation). This approach is faster but certainly less exact, and we recommend to use it only in case of prospective studies or non-detection results.

6 Statistical Analysis

6.1 Likelihood

We shall search for DM using a binned likelihood analysis[3] with bins in energy and spatial coordinates: data shall be binned in $N_{E'}$ E' bins (denoted by $\Delta E'_i$), by default, of equal size in a $\log E'$ scale and $N_{\bar{P}'}$ $\bar{P}'$ (or θ) bins (denoted by $\Delta \bar{P}'_j$ or $\Delta\theta_j$), with shape and size that optimize the sensitivity.

For each considered DM model (which specifies the DM particle mass plus the annihilation/decay spectrum dN/dE), we compute the profile likelihood ratio as a function of the free parameter α ($\alpha = \langle\sigma v\rangle$ for annihilation and $\alpha = 1/\tau_{\rm DM}$ for decay) [43]:

$$\lambda_P(\alpha \,|\, \boldsymbol{\mathcal{D}}) = \frac{\mathcal{L}(\alpha; \hat{\hat{\boldsymbol{\nu}}} \,|\, \boldsymbol{\mathcal{D}})}{\mathcal{L}(\hat{\alpha}; \hat{\boldsymbol{\nu}} \,|\, \boldsymbol{\mathcal{D}})} \quad , \tag{11}$$

where $\boldsymbol{\nu}$ represents the nuisance parameters and $\boldsymbol{\mathcal{D}}$ the data set; $\hat{\alpha}$ and $\hat{\boldsymbol{\nu}}$ are the values maximizing the likelihood function ($\mathcal{L}$), and $\hat{\hat{\boldsymbol{\nu}}}$ the value that maximizes $\mathcal{L}$ for a given value of α.

In the following we discuss two different likelihood functions that we recommend to use in CTA DM analyses, which basically differ in the way the residual background is estimated: the ON/OFF analysis (Section 6.1.1) and the global model fitting (Section 6.1.2). The former has the advantage of not needing an a-priori background model (with normally larger systematic uncertainties), whereas the latter may the only option for very extended or diffuse gamma-ray sources. In the future, different analyses can be proposed towards more accurate results, or for specific goals not covered by the present document. This shall be discussed and approved within the DMEP WG.

6.1.1 Background estimation from control (OFF) region

Whenever it is possible to define a background control (or OFF) region, where the expected background is the same as for the signal (or ON) region, we recommend to follow the approach described in Ref. [44],

[3] Unbinned versions of the likelihood functions shown below in this section can be also envisaged. However the computation time needed for the likelihood maximization process increases as the total number of events for the unbinned case and as the number of bins for the binned case. Given the large statistics expected in CTA DM analyses, we recommend in general the use of binned likelihood functions, and consider the use of unbinned likelihood functions only in cases where the gain of sensitivity with respect to the unbinned version justifies the increase in computation time.

with the likelihood function given by:

$$\begin{aligned}\mathcal{L}(\alpha;\boldsymbol{\nu}\,|\,\boldsymbol{\mathcal{D}}) \;=\; & \mathcal{L}(\alpha;\{b_{ij},\tau_{ij}\}_{i=1,...,N_{E'};j=1,...,N_{\bar{P}'}},J\,|\,\{N_{\mathrm{ON},ij},N_{\mathrm{OFF},ij}\}_{i=1,...,N_{E'};j=1,...,N_{\bar{P}'}}) = \\ & \mathcal{J}(J\,|\,J_{\mathrm{obs}},\sigma_J)\;\cdot \\ & \cdot\prod_{i=1}^{N_{E'}}\prod_{j=1}^{N_{\bar{P}'}}\frac{(g_{ij}(\alpha)+b_{ij})^{N_{\mathrm{ON},ij}}}{N_{\mathrm{ON},ij}!}e^{-(g_{ij}+b_{ij})}\frac{(\tau_{ij}b_{ij})^{N_{\mathrm{OFF},ij}}}{N_{\mathrm{OFF},ij}!}e^{-(\tau_{ij}b_{ij})}\;\cdot\;\mathcal{G}(\tau_{ij}\,|\,\tau_{\mathrm{obs}},\sigma_\tau)\quad,\end{aligned} \tag{12}$$

where, following the nomenclature defined in Section 2.1, g_{ij}, b_{ij} and $N_{\mathrm{ON},ij}$ are the estimated mean number of signal and background events, and the number of observed events, respectively, in the (i,j)-th ON bin; $N_{\mathrm{OFF},ij}$ is the number of observed events in the corresponding OFF bin (for prospective studies assumed to be $\frac{d\hat{b}}{dtdE'd\bar{P}'}$ integrated in the (i,j)-th bin and in T_{obs}); $\mathcal{J}$ is the likelihood for J, given measured $\log_{10}(J_{\mathrm{obs}})$ and its (statistical) uncertainty σ_J [34][4]:

$$\mathcal{J}(J\,|\,J_{\mathrm{obs}},\sigma_J)=\frac{1}{\ln(10)J_{\mathrm{obs}}\sqrt{2\pi}\sigma_J}\times e^{-\left(\log_{10}(J)-\log_{10}(J_{\mathrm{obs}})\right)^2/2\sigma_J^2}\quad; \tag{13}$$

τ_{ij} follows a Gaussian likelihood $\mathcal{G}$ with mean τ_{obs} (normally measured from the data), with a total uncertainty $\sigma_\tau\big(=\sqrt{\sigma^2_{\tau,\mathrm{stat}}+\sigma^2_{\tau,\mathrm{sys}}}$, with $\sigma_{\tau,\mathrm{sys}}=0.01$ as explained in Section 5.2$\big)$:

$$\mathcal{G}(\tau_{ij}\,|\,\tau_{\mathrm{obs}},\sigma_\tau)=\frac{1}{\sqrt{2\pi}\sigma_\tau}\times e^{-(\tau_{ij}-\tau_{\mathrm{obs}})^2/2\sigma_\tau^2}\quad. \tag{14}$$

(Note that there are $N_{E'}\times N_{\bar{P}'}$ independent τ_{ij} nuisance parameters, each associated to a given $\mathcal{G}$ term, all of which are described by single common τ_{obs} and σ_τ). b_{ij}, J and τ_{ij} are the nuisance parameters, whereas g_{ij} depend on the free parameter α through:

$$g_{ij}(\alpha)=T_{\mathrm{obs}}\int_{\Delta E'_i}dE'\int_{\Delta\bar{P}'_j}d\bar{P}'\int_0^\infty dE\int_{-\infty}^{\infty}d\Omega\,\frac{d\Phi(\alpha)}{dE\,d\Omega}\,A_{\mathrm{eff}}(E,\bar{P})\,f_E(E'\,|\,E,\bar{P})\,f_{\bar{P}}(\bar{P}'\,|\,E,\bar{P})\quad. \tag{15}$$

6.1.2 Global model fitting

An alternative approach to estimate the number of dark matter signal events present in our signal region consists in performing a global likelihood fit of all known contributions to our data sample, which will profit from the different expected spectral distribution and morphology of the different contributions [45]. This approach is indicated for those cases where a suitable OFF (background control) region cannot be defined, e.g. when studying the Galactic center region, due to the Galactic diffuse emission. In those situations we shall use the following likelihood function:

$$\begin{aligned}\mathcal{L}(\alpha;\boldsymbol{\nu}\,|\,\boldsymbol{\mathcal{D}}) \;=\; & \mathcal{L}(\alpha;\{\kappa_{ij}\}_{i=1,...,N_{E'};j=1,...,N_{\bar{P}'}},\{R_i^{\mathrm{CR}},R_i^{\mathrm{GDE}}\}_{i=1,...,N_{E'}},J\,|\,\{N_{ij}\}_{i=1,...,N_{E'};j=1,...,N_{\bar{P}'}}) \\ & =\mathcal{J}(J\,|\,J_{\mathrm{obs}},\sigma_J)\;\cdot \\ & \cdot\prod_{i=1}^{N_{E'}}\mathcal{R}(R_i^{\mathrm{CR}}\,|\,R_{\mathrm{min}}^{\mathrm{CR}},R_{\mathrm{max}}^{\mathrm{CR}})\,\mathcal{R}(R_i^{\mathrm{GDE}}\,|\,R_{\mathrm{min}}^{\mathrm{GDE}},R_{\mathrm{max}}^{\mathrm{GDE}})\;\prod_{j=1}^{N_{\bar{P}'}}\frac{\mu_{ij}^{N_{ij}}}{N_{ij}!}e^{-\mu_{ij}}\,\mathcal{G}(\kappa_{ij}\,|\,1,\sigma_\kappa)\quad,\end{aligned}$$

where:

$$\mu_{ij}=\kappa_{ij}\left(g_{ij}(\alpha)+R_i^{\mathrm{CR}}b_{ij}^{\mathrm{CR}}+R_i^{\mathrm{GDE}}b_{ij}^{\mathrm{GDE}}\right) \tag{16}$$

and N_{ij} are, respectively, the total expected and observed number of events, in the (i,j)-th bin; the terms κ_{ij} allow to account for systematic uncertainties produced by unmodeled variations in the exposure between the different $(E',\bar{P}')$ bins [45], and follow a Gaussian likelihood ($\mathcal{G}$, see Equation 14) with mean 1 and width $\sigma_\kappa=0.01$ (i.e. coherently with the systematic uncertainty in the background estimation as described in Section 5.2); the terms R_i^{X} parametrize the statistical and systematic uncertainties in the relative spectral shape of the different background contributions, and are described by step function likelihoods:

$$\mathcal{R}(R\,|\,R_{\mathrm{min}},R_{\mathrm{max}})=\begin{cases}\frac{1}{R_{\mathrm{max}}-R_{\mathrm{min}}} & \mathrm{if}\,R\in[R_{\mathrm{min}},R_{\mathrm{max}}]\\ 0 & \mathrm{otherwise}\end{cases}\quad, \tag{17}$$

[4] Other distributions of J, e.g. an asymmetric Gaussian, can be implemented if more realistic.

where, according to Ref. [45], $[R^{\rm CR}_{\rm min}, R^{\rm CR}_{\rm max}] = [0.5, 1.5]$ and $[R^{\rm GDE}_{\rm min}, R^{\rm GDE}_{\rm max}] = [0.2, 5]$ (in order to allow for a variability of a few); $\mathcal{J}$ is given by Equation 13; $g_{ij}(\alpha)$ is given by Equation 15; and $b^{\rm CR}_{ij}$ and $b^{\rm GDE}_{ij}$ (fixed parameters) are, respectively, the expected number of cosmic ray (CR) and galactic diffuse emission (GDE) background events expected in the (i,j)-th bin (labels "CR" and "GDE" will be referred to collectively in what follows as "X"), according to their respective models, and given by:

$$b^{\rm X}_{ij} = T_{\rm obs} \int_{\Delta E'_i} dE' \int_{\Delta \bar{P}'_j} d\bar{P}' \int_0^\infty dE \int_{-\infty}^\infty d\Omega \, \frac{d\Phi^{\rm X}(\alpha)}{dE\, d\Omega} \, A^{\rm X}_{\rm eff}(E, \bar{P}) \, f^{\rm X}_E(E' \,|\, E, \bar{P}) \, f_{\bar{P}}{}^{\rm X}(\bar{P}' \,|\, E, \bar{P}) \quad , \quad (18)$$

which follows the notation of Equation 15 but replacing gamma-ray flux and IRF functions by those for process "X". Note that IRFs for CR-type background events are in general very different from those for gamma-ray events, and would need to be computed (they are not normally part of the IRF), hence useful models should provide directly the values of $b^{\rm CR}_{ij}$.

6.2 Results

The **statistical significance of a putative signal** shall be quantified by the values $-2\ln\lambda_P$ for the no-signal (or null) hypothesis (H_0: $\alpha = 0$)). In first approximation, given a data set $\boldsymbol{\mathcal{D}}$, $\sqrt{-2\ln\lambda_P(\alpha = 0 \,|\, \boldsymbol{\mathcal{D}})}$ is the significance in equivalent Gaussian standard deviations (or "σ") for the detection of a gamma-ray signal. We shall claim a signal detection when $-2\ln\lambda_P(\alpha = 0 \,|\, \boldsymbol{\mathcal{D}}) \geq 25$. Given the relevance of such a claim we must: i) make sure that all systematic uncertainties in background estimation are properly included in the likelihood analysis, as described in Sections 5.2 and 6.1; and ii) consider the possibility that the detected signal may come from yet unidentified DM-unrelated processes.

In case of positive signal detection, and assuming a DM origin, we shall determine 1σ (or 68% confidence level, CL) **confidence contour** in the $(\alpha, m_{\rm DM})$ plane (under a certain assumption for the decay/annihilation channels) as the isocurve defined by $-2\ln\lambda_P(\alpha, m_{\rm DM} \,|\, \boldsymbol{\mathcal{D}}) = 2.30$ (where $m_{\rm DM}$ is also let as a free parameter). For a given fixed value of $m_{\rm DM}$, the 68% CL **confidence interval** for α is given by the solutions of $-2\ln\lambda_P(\alpha \,|\, \boldsymbol{\mathcal{D}}) = 1$. For other confidence levels see the corresponding thresholds in the Table 38.2 in the PDG review [43].

In case of no positive detection, we shall produce 1-sided 95% CL **upper limits** to α by solving the equation $-2\ln\lambda_P(\alpha) = 2.71$ (the largest of the two possible solutions), with α restricted to the physical region (i.e. $\alpha \geq 0$).

For prospective studies, we shall compute the **sensitivity**, defined as the median of the distribution of α upper limit values obtained from $O(300)$ null hypotheses analysis realizations. For each realization, the data samples shall be generated by randomly selecting independent $N_{{\rm ON},ij}$ and $N_{{\rm OFF},ij}$ according to a Poisson PDF with mean obtained from $\frac{d\hat{b}}{dt dE' d\bar{P}'}$ integrated in the relevant (E', $\bar{P}'$) bin and $T_{\rm obs}$. In addition, in each realization $\tau_{\rm obs}$ shall be replaced by an independent random value selected from the PDF in Equation 14. It is also recommended to produce 1- and 2-σ CL bands for the sensitivity, defined by the [15.9,84.1] and [2.3,97.7] percentile intervals of the α upper limit distribution, and plot them together with the upper limits and sensitivity (the popularly known as "Brazilian plot").

As a validation check, a faster way to compute the sensitivity consists in computing the α upper limit from the "Asimov data set", i.e. the one obtained by setting the observed number of events at each bin equal to the number of expected counts in the case of no DM signal and all nuisance parameters fixed at their expected mean value.

Both in the case of real data analysis and prospective studies, we should explore the possibility of releasing (in addition to confidence intervals and/or limits to the different DM physical parameters mentioned above) the values of $-2\ln\lambda_P$ vs. gamma-ray flux in energy bins, as done e.g. by the Fermi-LAT Collaboration [34]. This would allow any external scientist to compute their own results using CTA observations for any arbitrary DM model of their choice.

7 Analysis code

The main guideline regarding analysis codes is that the results of analysis should be reproducible. Thus, it is advised to use standard packages, e.g. `ctools` or `gammapy`. Different analysis codes can be used and should be discussed within the DMEP WG, e.g. on https://portal.cta-observatory.org/WG/PHYS/SitePages/Dark%20Matter%20and%20Exotic%20Physics%20SWG.aspx. Such codes should preferably be made public within the WG to guarantee the possibility of being reproduced.

References

[1] J. Hinton (Ed.) "CTA Science Case TDR", 2015. Available at https://portal.cta-observatory.org/WG/PHYS/SiteAssets/SitePages/Home/Science-Case-TDR.pdf

[2] P. Ciafaloni, D. Comelli, A. Riotto, F. Sala, A. Strumia and A. Urbano, JCAP **1103** (2011) 019

[3] L. Bergstrom, T. Bringmann, M. Eriksson and M. Gustafsson, Phys. Rev. Lett. **94** (2005) 131301

[4] T. Bringmann, L. Bergstrom and J. Edsjo, JHEP **0801** (2008) 049

[5] L. Bergstrom, T. Bringmann, M. Eriksson and M. Gustafsson, Phys. Rev. Lett. **95** (2005) 241301

[6] T. Bringmann, A. J. Galea and P. Walia, Phys. Rev. D **93** (2016) 043529

[7] M. Cirelli et al. J. Cosmol. Astropart. P. **1103** (2011) 051. See also http://www.marcocirelli.net/PPPC4DMID.html, release 5.0

[8] P. Ciafaloni et al. J. Cosmol. Astropart. P. **1103** (2011) 019

[9] T. Bringmann, F. Calore, A. Galea and M. Garny, JHEP **1709** (2017) 041

[10] J. A. R. Cembranos, A. de la Cruz-Dombriz, V. Gammaldi, R. A. Lineros and A. L. Maroto, JHEP **1309** (2013) 077

[11] F. Iocco and M. Benito, Phys. Dark Universe **15** (2017) 90

[12] J. F. Navarro, C. S. Frenk, and S. D. White, Astrophys. J. **462** (1996) 563.

[13] J. Einasto, Trudy Astrofizicheskogo Instituta Alma-Ata **5** (1965) 87

[14] J. F. Navarro et al. Mon. Not. R. Astron. Soc. **349** (2004) 1039

[15] J. N. Bahcall and R. M. Soneira Astrophys. J. Suppl. S., **44** (1980) 73

[16] P. Ullio and M. Valli J. Cosmol. Astropart. P. **1607** (2016) 025

[17] K. Hayashi et al. Mon. Not. R. Astron. Soc. **461** (2016) 2914

[18] N. Bernal, L. Necib and T. R. Slatyer J. Cosmol. Astropart. P. **1612** (2016) 030

[19] M. Pato, O. Agertz, G. Bertone, B. Moore, and R. Teyssier, Physics Review D **82** (2010) 023531

[20] A. Moliné et al. Mon. Not. R. Astron. Soc. **466** (2017) 4974

[21] T. Bringmann, New Journal of Physics, **11** (2009) 105027

[22] L. Pieri et al. Phys. Rev. **D83** (2011) 023518

[23] A. Di Cintio et al. Mon. Not. R. Astron. Soc. **437** (2014) 415

[24] M. Ackermann et al. Phys. Rev. **D91** (2015) 122002

[25] A. Abramowski et al. Phys. Rev. Lett. **106** (2011) 161301

[26] H. Abdallah et al. Phys. Rev. Lett. **117** (2016) 111301

[27] M. Pato, F. Iocco and G. F. Bertone J. Cosmol. Astropart. P. **1512** (2015) 012

[28] V. Bonnivard et al. Mon. Not. Roy. Astron. Soc. **453** (2015) 849.

[29] G. D. Martinez, Mon. Not. Roy. Astron. Soc. **451** (2015) 2524.

[30] V. Bonnivard et al. Comput. Phys. Commun. 200 (2016) 336

[31] A. Chiappo et al. Mon. Not. R. Astron. Soc. **466** (2017) 669

[32] K. Ichikawa et al. MNRAS submitted (2017). arXiv:1706.0581

[33] K. Ichikawa et al. Mon. Not. Roy. Astron. Soc. **468** (2017) 2884

[34] M. Ackermann et al., Phys. Rev. Lett. **115** (2015) 231301

[35] M. Ahnen et al. J. Cosmol. Astropart. P. **1602** (2016) 039

[36] A. Klypin et al. Mon. Not. R. Astron. Soc. **457** (2016) 4340

[37] M. Ackermann et al. Astrophys. J. **812** (2015) 159

[38] N. Okabe et al. Astrophys. J. **784** (2014) 90

[39] P. Marchegiani and S. Colafrancesco, J. Cosmol. Astropart. P. **1611** (2016) 033

[40] A. Tamm et al. Astron. Astrophys. **546** (2012) A4

[41] G. Maier et al. "Description of CTA Instrument Response Functions (Production 3b Simulation)", https://forge.in2p3.fr/projects/cta_analysis-and-simulations/repository/entry/DOC/InternalReports/IRFReports/released/v1.1/cta-aswg-IRFreport.pdf.

[42] https://jama.cta-observatory.org/perspective.req#/items/3274?projectId=6

[43] K. A. Olive et al., Chin. Phys. **C38** (2014) 090001. Available at http://pdg.lbl.gov/2015/reviews/rpp2014-rev-statistics.pdf

[44] J. Aleksić, J. Rico and M. Martinez, J. Cosmol. Astropart. P. **1210** (2012) 032

[45] H. Silverwood et al. J. Cosmol. Astropart. P. **1503** (2015) 055